Plant-specific ribosome biogenesis factors in *Arabidopsis thaliana* with essential function in rRNA processing

Denise Palm[1], Deniz Streit[1], Thiruvenkadam Shanmugam[1], Benjamin L. Weis[1], Maike Ruprecht[1], Stefan Simm[1,2] and Enrico Schleiff [1,2,3,*]

[1]Institute for Molecular Biosciences, Goethe University Frankfurt, Max von Laue Str. 9, D-60438 Frankfurt, Germany, [2]Frankfurt Institute for Advanced Studies, D-60438 Frankfurt, Germany and [3]Buchmann Institute for Molecular Life Sciences, Goethe University Frankfurt, D-60438 Frankfurt, Germany

ABSTRACT

rRNA processing and assembly of ribosomal proteins during maturation of ribosomes involve many ribosome biogenesis factors (RBFs). Recent studies identified differences in the set of RBFs in humans and yeast, and the existence of plant-specific RBFs has been proposed as well. To identify such plant-specific RBFs, we characterized T-DNA insertion mutants of 15 *Arabidopsis thaliana* genes encoding nuclear proteins with nucleotide binding properties that are not orthologues to yeast or human RBFs. Mutants of nine genes show an altered rRNA processing ranging from inhibition of initial 35S pre-rRNA cleavage to final maturation events like the 6S pre-rRNA processing. These phenotypes led to their annotation as 'involved in rRNA processing' - *IRP*. The *irp* mutants are either lethal or show developmental and stress related phenotypes. We identified IRPs for maturation of the plant-specific precursor 5′-5.8S and one affecting the pathway with ITS2 first cleavage of the 35S pre-rRNA transcript. Moreover, we realized that 5′-5.8S processing is essential, while a mutant causing 6S accumulation shows only a weak phenotype. Thus, we demonstrate the importance of the maturation of the plant-specific precursor 5′-5.8S for plant development as well as the occurrence of an ITS2 first cleavage pathway in fast dividing tissues.

INTRODUCTION

Ribosome biogenesis is an essential process in which pre-ribosomal RNAs of the pre-40S and pre-60S particles are processed to form mature 80S ribosomes consisting of the small 40S and large 60S ribosomal subunit (1). The nascent 35S pre-rRNA transcript within the 90S pre-ribosomal particle is transcribed by RNA-Polymerase I in the nucleolus. The polycistronic transcript contains the 18S, 5.8S and 25S pre-rRNAs separated by two internal transcribed spacers (ITS1, ITS2) and flanked by two external transcribed spacers (5′-ETS, 3′-ETS, (2)). The 5S pre-rRNA is synthesized independently by RNA-polymerase III in the nucleus.

The mature 40S ribosomal subunit comprises the 18S rRNA and 33 ribosomal proteins, whereas the 60S ribosomal subunit contains the 25S, 5.8S and 5S rRNAs and 47 ribosomal proteins. The ribosome assembly and processing is best described for *Saccharomyces cerevisiae* (3,4). Today, the regulation of rRNA modification and hypermodification (5), the role of non-coding RNAs (6), the rRNA folding events (7) and structural constrains of the pre-ribosomal particles have been largely explored based on fungal model systems (8–16). Recent large scale bioinformatics and experimental studies expanded our knowledge on the fundamental processes of ribosome biogenesis in archaea (17–19), humans (20–23) and plants (18,19,24). The process has been linked to many human diseases (25,26) and to nucleolar stress in humans and plants (27,28). In addition, functional ribosome biogenesis is important for plant developmental and growth processes (29–31), salt stress responses (32) and the regulation of sugar metabolism (33–34).

The analysis of ribosome biogenesis in plants revealed two alternative processing pathways co-existing in plants (2,35). Pathway 1 starts with the 5′-ETS removal followed by the ITS1 cleavage which leads to the separated assembly of the pre-40S and pre-60S ribosomal subunit (2). This pathway is comparable to the yeast rRNA processing way. Pathway 2 is initiated by ITS1 cleavage and subsequent removal of the 5′-ETS, which is comparable to the human processing pathway. Furthermore, specific precursors like the

5′-5.8S pre-rRNA have been identified as plant-specific intermediates in the rRNA processing pathway (29,30,36).

The rRNA maturation and modification depends on a multitude of ribosome biogenesis factors (RBFs) and small nucleolar RNAs (snoRNAs). For yeast, 255 RBFs associated with rRNA processing are described (3). However, only ∼70% of yeast RBFs could be assigned in orthologous groups together with plants proteins (18,19). Moreover, a large scale screening in humans documented that human genes orthologous to yeast RBFs are not always involved in ribosome biogenesis in humans, while proteins known to act in pathways distinct from ribosome biogenesis can act as RBFs as well (23).

Consequently, the analysis of plant-specific RBFs is central to understand the process and the regulation of ribosome biogenesis in plants. In support of this notion regulation of ribosome biogenesis has been linked to plant-specific signaling and stress response events. It has been demonstrated that regulation of ribosome biogenesis is interlinked with cellular regulation by the phytohormone auxin (31,37–39). Auxin induces - among others - cell elongation and division, both requiring a rapid increase of the proteome and thus, relying on functional ribosomes. A similar link can be established with respect to stress responses that are accompanied by massive alterations of the transcriptome and subsequently the proteome to cope with the new environmental situations. It has been demonstrated that plants with affected ribosome biogenesis are less efficient in stress response and show severe phenotypes, e.g. under cold, salt or metabolite stress (27,32,33,38). Thus, the description of the inventory required for plant ribosome maturation is paramount to link this important process to physiological behavior of plants.

Among the identified and characterized RBFs in *Arabidopsis thaliana* many factors are orthologous to yeast RBFs (2,40,41; and references therein). In addition, plant RBFs orthologous to yeast RBFs encoded by at least two independent genes (1:n) have been identified. On the one hand, an overlapping function in ribosome biogenesis of both plant genes was observed, e.g. in case of Brx1 (36). On the other hand, distinct functionalities of the different co-orthologues have been described. For example, only one co-orthologue of Lsg1 is essential for ribosome biogenesis, while the second co-orthologue most likely performs an alternative function (42). Moreover, several plant proteins not being orthologous to yeast or human RBFs have been identified to be involved in rRNA processing and ribosome biogenesis, for example the G-patch domain protein GDP1 (43), Pum23 (44) and APUM24 (27,45).

Remarkably, multiple nucleotide binding proteins without orthologues to yeast or human RBFs have been identified in the proteome of the nucleus and nucleolus (24,46,47), but their function remains largely unknown. As the identification of proteins specifically involved in plant ribosome biogenesis is important to initiate an understanding of plant-specific regulatory events, we characterized 15 nuclear plant proteins that are not orthologous to yeast or human RBFs. Six of these proteins are conserved in eukaryotes, but

their function has not been related to ribosome biogenesis. By screening corresponding T-DNA insertion mutants we identified nine factors with a function important for efficient rRNA processing in plants, six of them without an orthologue in yeast or human in general. The mutation of the selected factors by T-DNA insertion leads to lethality or severe growth defects. In addition, the response to auxin or glucose treatment as well as the tolerance to salinity stress is altered when compared to wild-type plants. These phenotypes led to the annotation of the proteins as 'involved in rRNA processing' - *IRP*.

Strikingly, while both a 5′ extended (5′-5.8S) and a 3′ extended (6S) precursor of the 5.8S have been identified in plants, we observed that maturation of the 5′-5.8S pre-rRNA is essential and cannot be bypassed by the pathway utilizing the 6S pre-rRNA. Moreover, we identified a mutant in which an intermediate P-C$_2$ accumulates upon auxin treatment indicative of an ITS2-first processing pathway. Subsequent analysis of rRNA processing intermediates in fast dividing cell cultures uncovered the existence *in vivo* as well. Thus, a second plant-specific pre-rRNA intermediate exists beside the 5′-5.8S.

MATERIALS AND METHODS

Orthologue search and domain architecture analysis

The orthologue search between yeast, human and *A. thaliana* for identification of orthologous groups containing proteins known to function as RBFs based on literature (18,19) was performed via HaMStR and OrthoMCL as previously described (24). For the additional information about the orthologous groups in Viridiplantae the orthologue search via OrthoMCL (48) and InParanoid (49) was performed using proteomes of 61 plant-species available from the phytozome (50). Based on the pangenome of the Viridiplantae including the orthologous groups we defined the earliest occurrence of the IRPs in the Viridiplantae. The OMA browser (51) was used to identify orthologues in all kingdoms of organisms (Supplemental Table S1) down to LUCA to verify the results of our pangenome of Viridiplantae and include the possibility to detect the ancestor of the IRPs in the whole tree of life.

The domain architecture of the protein sequence was analyzed using Pfam (February 2017 (52)) and Prosite (February 2017 (53)) databases. The profile Hidden-Markov-Models (pHMMs) were used via HMMER (54) to align domains and functional motifs on the protein sequences. We restricted the domains to putative nucleotide binding motifs and compared our findings with the domain annotation of Aramemnon (55). Information about the genes and proteins was extracted from Aramemnon and TAIR10 (56).

Construct generation

CDS of each RBF candidate was amplified by RT-PCR using *A. thaliana* derived cDNA as described (29) with oligonucleotides listed in Supplemental Table S2. The CDS was cloned in the pRTds-GFP vector by the method previously described (24,42).

Protoplast isolation, transformation and analysis of fluorescence

Protoplast isolation and transformation was done as previously described (29,57). In brief, leaves of 4-week-old *A. thaliana* (short day conditions) were rubbed over sandpaper and transferred into glass dishes with MCP (500 mM sorbitol, 1 mM CaCl$_2$, 29 mM MES) supplemented with BSA. The entire procedure takes about 20 min. Supernatant was removed and exchanged for enzyme solution (1% cellulase and 0.3% macerozyme in 20 ml MCP) and the leaves were incubated for 2 h at 30°C. For release of protoplasts, petri dish was gently shaken for a minute, subsequently filtered through a 75 μm nylon mesh and underlaid with MCP in 100% Percoll. After centrifugation at 405 g for 8 min at RT, supernatant was removed, protoplasts mixed with the residual Percoll and a second gradient was formed by addition of 25 and 0% Percoll in MCP. After centrifugation at 270 g for 8 min at RT, intact protoplasts were collected from the interphase between 25 and 0% Percoll layer, pelleted and adjusted to 10^6 protoplasts/ml in MMG solution (400 mM sorbitol, 15 mM MgCl$_2$, 5 mM MES). For transformation, 10^5 protoplasts were co-transformed with 10 μg of pRTds-GFP and 10 μg AtFib2-mCherry vectors.

After 8 hours of protein expression, GFP-fluorescence (excitation at 488 nm, emission at 505–525 nm) and mCherry-fluorescence (excitation at 568 nm, emission 580–610 nm) were analyzed by confocal laser-scanning microscopy using a Leica SP5 as previously defined (24,57). The nucleolar localization of the protein of interest was concluded form the overlay of the mCherry and GFP-fluorescence. The nuclear localization was concluded from both, the vicinity of GFP-fluorescence to the mCherry fluorescence and the overlay of the GFP-fluorescence with the bright filed image (not shown).

T-DNA insertion plant lines

The T-DNA insertion lines were obtained from Nottingham Arabidopsis Stock Center (NASC); with the nomenclature given in Table 2 & Supplemental Table S3. Genomic DNA preparation from leaves or flowers was done as described (58). T-DNA insertions were mapped as established (59). For analysis of the zygosity of the appropriate T-DNA, PCR on isolated gDNA was performed using the T-DNA left border oligonucleotide together with either the reverse or the forward genomic primers (Supplemental Table S4; (29)). The observed position of the different T-DNA insertions is presented in Supplemental Figure S1. Screening for homozygosity was performed in T1 and T2, while T3 was used for further analysis.

Cultivation of plants on soil and plates

Seeds of T-DNA insertion lines were either directly sown on soil or for further analysis placed on plates containing $\frac{1}{2}$ MS-medium with or without appropriate antibiotics for selection. For phenotypic analysis plants were cultivated on soil in growth chambers under long day conditions (14/10h light/dark cycles at 21/18°C). For analysis of germination rate and stress conditions, seeds were surface sterilized by adding 6% sodium-hypochlorite for 1–2 min, followed by 70% ethanol for 1–2 min and subsequent five washes with double distilled water. For synchronization of germination, seeds were stratified for five days at 4°C in the dark and cultivated under short day conditions (8/16 h light/dark cycles at 21–18°C).

Northern Blot analysis and rRNA sequencing

RNA isolation from 14-day-old *A. thaliana* seedlings was performed as described (42,60). For isolation of RNA from root cell cultures by the same method, *A. thaliana* root cell culture was grown as described (24). Pelleted cells were ground using liquid nitrogen and RNA isolated as described for seedlings. Pre-rRNAs were separated by RNA gel electrophoresis and detected by northern blotting as established (29,42,61) with probes listed in supplemental Table S5. For analysis of large rRNAs 1.2% agarose gel was used, while small rRNAs were analyzed on 8% urea-polyacrylamide gels.

rRNA intermediate sequencing was performed as described in (45). Briefly, 1 μg of Arabidopsis root cell culture RNA was circularized using T4 RNA Ligase I (NEB), with which reverse transcription was performed using 18S-specific cRT oligo. The circular complementary DNA was used as template for PCR reaction using oligos cRT-F and cRT-R binding in outward facing orientation (Supplemental Table S5). The amplified product was subsequently cloned in TA vector and sequenced in high copy numbers to reflect intermediate variations.

Analysis of the T-DNA insertion plant lines

For analysis of the germination rate 100 seeds were sown on MS-plates without antibiotics and kept under short day conditions. After six days the ratios between germinated to non-germinated were calculated. Growth stage analysis was performed according to (62). Statistical significance of difference was tested by ANOVA.

Visualization of embryos in seeds was performed as described previously (63): siliques of the same developmental stage were excised from wild-type and T-DNA insertion lines and first incubated in 9:1 ethanol: acetic acid solution overnight at room temperature, followed by incubation for 1 h in 90% ethanol and storage in 70% ethanol. Seeds were photographed using the inverted Olympus CKX41 microscope.

Treatment of T-DNA insertion lines

Auxin treatment was performed by supplementation of half-strength MS-medium with 10 μM auxin. Seedlings were harvested 14 days after germination and further used for RNA extraction. For salt treatment half-strength MS-medium was supplemented with 100 mM NaCl and seedlings were photographed 25 days after germination.

For glucose treatment, half strength MS-medium was supplemented with 200 mM glucose and seedlings were photographed 25 days after germination. All stress treatments were performed in growth chambers under short-day conditions.
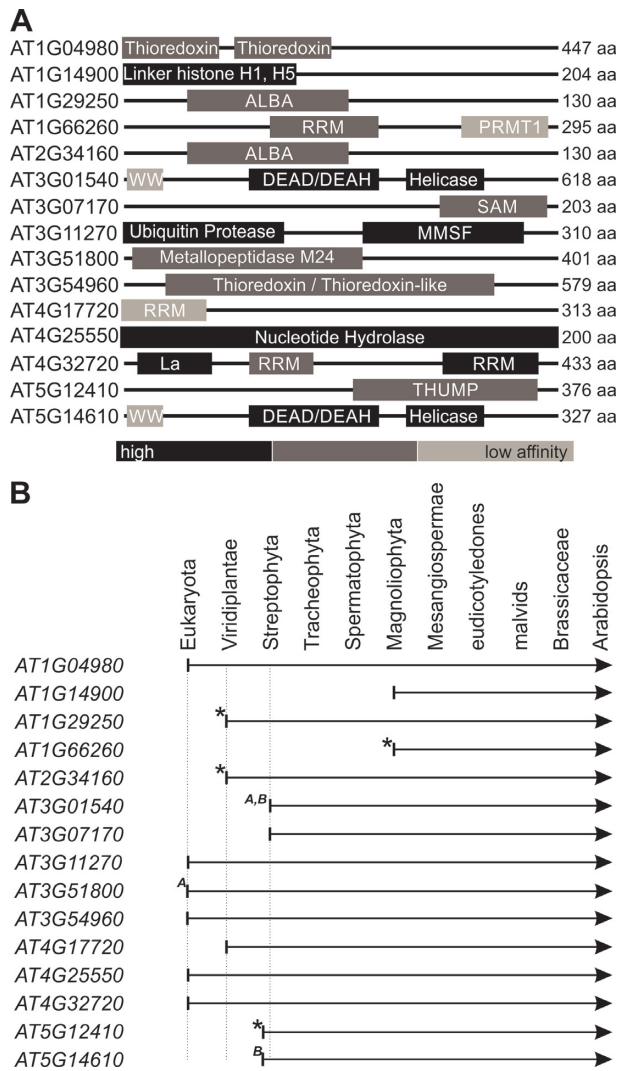
Figure 1. Properties and occurrence of proteins identified in the nuclear or nucleolar fraction by proteomic approaches. (**A**) The domain structure of the 15 selected proteins is shown. The nomenclature is: ALBA, acetylation lowers binding affinity domain of an archaeal chromosomal protein; La, motif adopts an alpha/beta fold that comprises a winged-helix motif; MMSF, Maintenance of mitochondrial structure and function; PRTM1, C-terminal duplication domain of Friend of PRMT1; RRM, RNA recognition motif; SAM, sterile α motif; WW, rsp5-domain or WWP repeating motif. (**B**) The evolutionary occurrence of the genes coding for the 15 proteins is shown.

Accession numbers

All accession numbers are listed in Table 1.

RESULTS

Domain organization of putative nuclear or nucleolar plant proteins

We analyzed 15 proteins with a putative nucleotide binding domain that have been identified by proteomics in the nucleolar or nuclear fraction after cell fractionation (24,47). AT1G04980 and AT3G54960 contain predicted thioredoxin domains (Figure 1A) found e.g. in proteins with RNA chaperone activity (64). AT1G14900 contains

a linker histone (H1, H5) domain (65). AT1G29250 and AT2G34160 have a predicted 'acetylation lowers binding affinity' (ALBA) domain characterizing RNA binding proteins and both proteins are co-orthologues (66). AT1G66260, AT4G17720 and AT4G32720 contain a RNA recognition motif (RRM; (67)) and AT4G32720 a La-domain known to bind RNA (La; 68). The AT3G01540 and AT5G14610 have a WW-domain and domains characteristic of e.g. helicases (DEAD/DEAH; 69). Moreover, both proteins are co-orthologous. AT3G07170 encodes a protein with an RNA binding domain called sterile α motif (SAM) (70,71). AT3G11270 has a ubiquitous protease domain and a domain that marks the protein as a proteasomal subunit (72). AT3G51800 is characterized by the metallopeptidase domain M24 that was found e.g. in transcription factor subunits (73), while AT4G25550 contains a nucleotide hydrolase domain found e.g. in enzymes involved in polyadenylation (74). AT5G12410 contains a so called THUMP (after thiouridine synthases, RNA methylases and pseudouridine synthases) domain found in RNA modifying enzymes (75).

The proteins selected are not in an orthologous group with yeast or human RBFs. Orthologues of six of the proteins are found in all eukaryotes (Figure 1B; Supplemental Table S1; AT1G04980, AT3G11270, AT3G51800, AT3G54960, AT4G25550, AT4G32720). Three proteins have orthologues in all orders of the analyzed Viridiplantae (AT1G29250; AT2G34160; AT4G17720). Based on our analysis four proteins have orthologous sequences in Streptophyta (AT3G01540, AT3G07170, AT5G12410, AT5G14610) and two in Magnoliophyta only (AT1G14900, AT1G66260). In the orthologous groups containing AT1G29250, AT1G66260, AT2G34160 and AT5G12410 sequences sporadically occur in other eukaryotic species like Leishmania, Naegleria, Galdieria or Leptomonas species as well as the fungi species of Aspergillus, but their distribution does not suggest a general occurrence in all eukaryotes (Figure 1B asterisk, Supplemental Table S1). Similarly, we identified some sequences from archaea in the orthologous group containing AT3G01540 and AT3G51800 as well as from bacteria in the orthologous group containing AT3G01540 and AT5G14610. Again, the occurrence of these sequences does not support a global existence in these branches via OMA and the hierarchical orthologous groups. Nevertheless, it might well be that these proteins originated from bacterial ancestors.

Cellular localization of putative nuclear or nucleolar plant proteins

To further support the annotated localization of the selected proteins inferred from proteomics (24,47), we generated fusion proteins with N- or C-terminal GFP. We approached the fusion at both termini to avoid masking a specific terminal localization signal or motif for complex formation. All fusion proteins were co-expressed in *A. thaliana* mesophyll protoplasts with the nucleolar marker atFIB2-mCherry (e.g. 29) to determine the intracellular localization. Note, this approach yields an overexpression which might in part enforce mis-localization in addition to proper cellular localization of the fusion protein. We analyzed GFP-fluorescence (Figure 2A, left), mCherry-fluorescence

Table 1. Localization of the proteins determined by GFP or by published proteomics

Gene	N-terminal GFP	C-terminal GFP	Palm (24)	Montacié (47)
AT1G04980	Cytosol/nucleus/nucleolus	Cytosol/nucleus/nucleolus	Cytosol/nucleus/nucleolus	-
AT1G14900	Nucleus/nucleolus	Nucleus/nucleolus	Cytosol/nucleus/nucleolus	-
AT1G29250	Cytosol	Cytosol	Nucleolus	-
AT1G66260	Nucleus/nucleolus	Nucleus/nucleolus	Nucleolus	Nucleolus
AT2G34160	Cytosol/nucleus	Cytosol	Nucleolus	-
AT3G01540	Nucleus/nucleolus	Nucleus/nucleolus	Nucleolus	Nucleolus
AT3G07170	Nucleus/nucleolus	Nucleus/nucleolus	Nucleus/nucleolus	Nucleolus
AT3G11270	Cytosol/nucleus	Cytosol/nucleus	Nucleus	-
AT3G51800	Cytosol/nucleus/nucleolus	Cytosol/nucleus	Cytosol/nucleus/nucleolus	Nucleolus
AT3G54960	Cytosol	n.d.	Cytosol/nucleus/nucleolus	-
AT4G17720	Cytosol	Cytosol/nucleus	Cytosol/nucleus	-
AT4G25550	Cytosol/nucleus	Cytosol/nucleus	Nucleus	-
AT4G32720	Nucleus	Nucleus	Cytosol/nucleolus	Nucleolus
AT5G12410	Nucleus	Nucleus	Cytosol/nucleus	-
AT5G14610	nucleus/nucleolus	Cytosol/nucleus/nucleolus	Nucleus/nucleolus	-

The results presented in figure two are presented. Note that Montacie *et al.* tested only for presence in nucleolus.

(Figure 2A, middle) and chlorophyll auto-fluorescence of chloroplasts (Figure 2A, right). In addition, the localization of the GFP-fluorescence was analyzed by overlay with the bright field image to distinguish between nuclear and nuclear/cytoplasmic localization (not shown). Based on these overlays of signals we conclude that AT1G66260 GFP-fusions show a nuclear and nucleolar localization.

GFP-fluorescence of AT1G29250 and AT3G54960 GFP-fusions was identified in cytosol (Figure 2B; Table 1), of AT4G32720 and AT5G12410 in the nucleus (Figure 2C; Table 1) and of AT2G34160, AT3G11270, AT4G17720 and AT4G25550 in both compartments (Figure 2D; Table 1). AT1G14900, AT3G01540 and AT3G07170 GFP-fusions expressed in protoplasts yielded GFP-fluorescence signals in the nucleus and nucleolus (Figure 2E; Table 1), while AT1G04980, AT3G51800 and AT5G14610 were identified in all three compartments (Figure 2F; Table 1). Worth mentioning, for AT4G17720, AT2G34160 and AT5G14610 we noticed variations for the N-terminal and C-terminal fusion with respect to the detection in the cytosol (Table 1).

These results obtained by assessment of the GFP-fluorescence were largely overlapping with the proteomic detection (24,47). However, for AT1G29250, AT2G34160 and AT3G54960 we observed a discrepancy between the localization of GFP-fluorescence microscopy and the identification by proteomics (Table 1). By proteomics, AT1G29250 and AT2G34160 were identified in the nucleolar fraction and AT3G54960 in all three analyzed compartments (24). In contrast, the GFP-fusion proteins of AT1G29250 and AT3G54960 were localized in the cytoplasm and the GFP-fusion protein of AT2G34160 in the cytoplasm and in the nucleus (Figure 2B). Worth mentioning, all three proteins have not been identified in the nucleolus by a subsequent proteome analysis of this compartment (47). Nevertheless, the cytosolic localization of the three proteins might reflect a partially dysfunctional population of the protein not properly assembled into the complexes.

Mutants of the selected genes show a differential impact on rRNA processing

For all 15 factors, we obtained available T-DNA insertion lines (Supplemental Figure S1). We confirmed the localiza-tion of T-DNA insertion by digestion and re-ligation of gDNA and subsequent sequencing of PCR products with T-DNA specific oligonucleotides (not shown). The zygotic state of the plant lines was analyzed by PCR with gDNA. For 12 lines a homozygous state was observed (Supplemental Figure S1), while only heterozygous mutant lines of *AT1G66260, AT4G17720, AT4G25550* and *AT4G32720* could be isolated (Supplemental Figure S1). The T3 generation of all lines (assuming that ordered lines have been T0), whether in homozygous or heterozygous state, were used for subsequent studies.

The rRNA processing in all mutant lines was analyzed by northern blots with established probes (Figure 3A, (29)) using ethidium bromide (EtBr) staining of mature rRNA as loading control. For mutants of *AT1G04980, AT1G14900, AT3G51800, AT3G54960, AT5G12410* or *AT5G14610* we did not observe drastic alterations of the pre-rRNAs levels (only quantification is shown; Figure 3C). In turn, for mutants of nine factors we observed alterations in the abundance of pre-rRNAs when compared to wild-type (Figure 3B). Based on the observed impact of these T-DNA insertion mutants on rRNA processing we assigned the according mutants as 'involved in rRNA processing' (*irp*).

The T-DNA insertion line of *IRP1* (*AT3G07170, irp1-1*) had a reduced level of 35S, while both, 35S and 33S pre-rRNAs were lower in heterozygote *IRP2* mutants (*AT4G32720, irp2-1* +/−, *irp2-2* +/−) than in wild-type (Figure 3B, C). In *irp3-1* +/− (*AT4G17720, IRP3*) 35S, 33S, and $27S\text{-}B_{S/L}$ pre-rRNAs are reduced. In turn, none of the other detected pre-rRNAs analyzed accumulated in the mutant plants. The T-DNA insertion in *IRP4* (*AT3G11270, irp4-1*; Figure 3B, C) resulted in decreased levels of the 35S and 33S pre-rRNAs and in a pronounced increase of the 5.8S+30 and 6S transcripts when compared to wild-type. In *irp5-1* and *irp5-2* (*AT1G29250, IRP5*; Figure 3B, C) the 33S pre-rRNA was enriched, which might link its function to the regulation of P_2 cleavage. The mutant of *IRP6* (*AT3G01540, irp6-1*) showed higher levels of $27S\text{-}A_2$ and $27S\text{-}A_3$ pre-rRNA. Mutants affecting the function of IRP7 (*AT2G34160, irp7-1*; Figure 3B, C) and IRP8 (*AT1G66260; irp8-1*) yielded in an increase of $27S\text{-}A_3$, $P\text{-}A_3$, $P'\text{-}A_3$ and $18S\text{-}A_3$ precursors when compared to wild-type. Further-
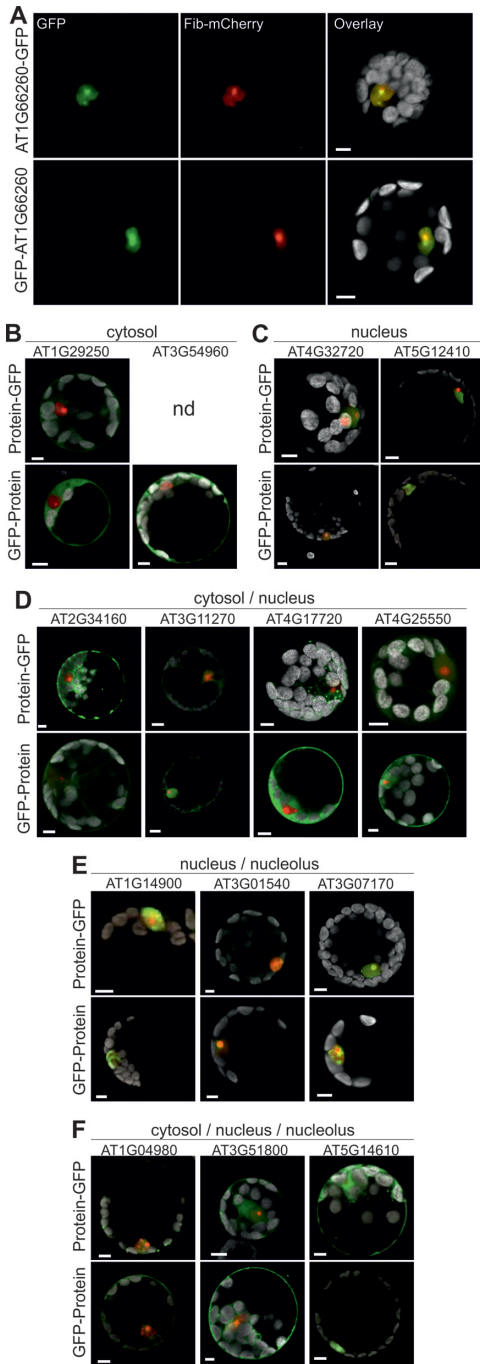
Figure 2. Localization of the investigated proteins. For each factor a plasmid coding for a fusion protein with C- or N-terminal GFP was transformed into protoplasts in combination with a plasmid coding for AtFib2-mCherry. The GFP- (green), mCherry- (red) and chlorophyll auto-fluorescence (white) was recorded. (**A**) The GFP-fluorescence (left), the mCherry-fluorescence (middle) and the overlay of GFP-, mCherry- and chlorophyll auto-fluorescence (right) for representative protoplasts transformed with AT1G66260-GFP (top) and GFP-AT1G66260 (bottom) is shown. (**B–F**) The overlay of GFP-, mCherry- and chlorophyll auto-fluorescence for representative protoplast transformed with indicated protein-GFP (top) and GFP-protein coding plasmids is shown (bottom). The proteins with localization in the cytosol (B), nucleus (C) cytosol and nucleus (D), nucleus and nucleolus (E) or cytosol, nucleus and nucleolus (F) are grouped. Protein integrity was probed by western blot analysis with GFP antibody (not shown). AT3G54960-GFP expression yielded free GFP and the results were omitted (nd).
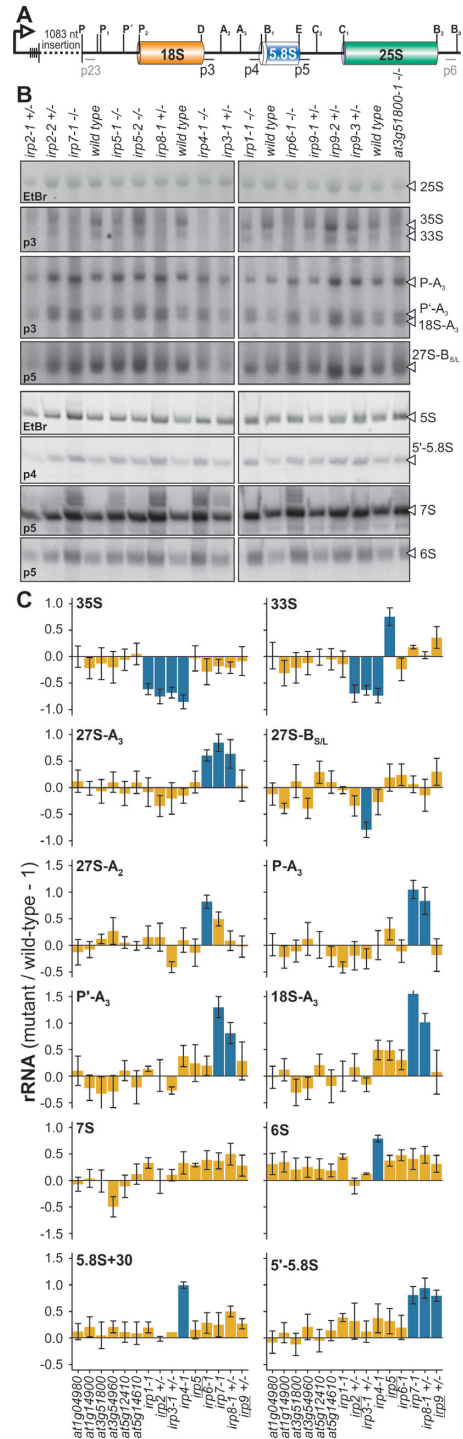
Figure 3. Analysis of the rRNA processing. (**A**) The rDNA gene model indicating the processing sites and annealing positions of the northern probes. In grey the annealing position of probes additionally used in Figure 5C are indicated. (**B**) Representative northern blots, with probes indicated (left), for T-DNA insertion lines with altered rRNA processing. The names of the rRNA intermediates are indicated (right). (**C**) Quantification of the intensities of different rRNA intermediates from multiple independent experiments (n>3). Values were normalized to ethidium bromide stained mature 25S and 18S rRNAs and are expressed as a ratio to the intensity observed in wild-type. The baseline is set to 1 and the standard deviation is shown as an error bar. In blue are all quantifications showing more than 50% increase or decrease in the mutant, and in orange are all below this threshold.

more, in *irp7-1 and irp8-1 +/−*, as well as in *irp9-1 +/−, irp9-2 +/− and irp9-3 +/− (AT4G25550; IRP9)*, 5′-5.8S pre-rRNA accumulated.

Thus, we identified four factors not orthologous to yeast or human RBFs affecting the synthesis or stability of the 35S and 33S (IRP1 to IRP4), two that influence maturation of 27S-A$_2$ and 27S-A$_3$ (IRP5, IRP6) and two important for 18S maturation (IRP7, IRP8). In addition, IRP4 seems to be required for 3′ maturation of the 5.8S. In turn, IRP7-IRP9 function is important for 5′-5.8S pre-rRNA processing or final quality control of ribosome biogenesis.

Mutants of *IRP*s show an altered growth behavior

We analyzed the phenotype of the T-DNA insertion mutants of IRPs. For all mutants confirmed to be homozygous, germination rate is comparable to that of the wildtype (Figure 4A, *irp −/−*). Consistent with a lethal phenotype, germination rate of mutants of *IRP2 (irp2-1 +/−* and *irp2-2 +/−)*, *IRP8 (irp8-1 +/−)* and *IRP9 (irp9-1 +/−, irp9-2 +/− and irp9-3 +/−)* was reduced by at least 25% when compared to wild-type (Figure 4A). This is in agreement with the highest expression of *IRP2* in the embryo of the pre-globular, globular and heart stage and of *IRP8* in late development stages of seeds (Supplemental Figure S2; (76,77)) and mature pollen (Supplemental Figure S3; (76)). The expression of the gene coding for IRP9 is high in the pre-globular and heart stage (Supplemental Figure S2; (76)). The most drastic effect on germination was observed for *irp3-1 +/−*, for which a germination rate of only 25% in comparison to wild-type was observed (Figure 4A). Consistent with this observation, the expression of the according gene is highest in the embryo, the endosperm of developing seeds (Supplemental Figure S2; (76,77)) and mature pollen (Supplemental Figure S3; (76)).

The rate of leaf development was comparable between mutants of *IRP1, IRP4, IRP5, IRP6, IRP7, IRP8* and wildtype (Figure 4B, 1.02, 1.06, 1.12). In contrast, *irp2-1 +/−, irp2-2 +/−, irp3-1 +/−, irp9-1 +/−, irp9-2 +/−* and *irp9-3 +/−* showed a reduced developmental rate when compared to wild-type (Figure 4B, 1.02, 1.06, 1.12). In addition, plants of these six lines were smaller than wild-type plants and mutants of *IRP9* showed a chlorotic phenotype (Figure 4C).

Development of the inflorescence was delayed in case of *irp5-1, irp5-2, irp7-1 +/−, irp8-1 +/−, irp9-1 +/−, irp9-2 +/−* and *irp9-3 +/−* when compared to wild-type (Supplemental Figure S4). Further, we observed a reduced growth of the inflorescence for *irp1-1* and *irp3-1 +/−*, but a longer inflorescence for *irp4-1* (Supplemental Figure S4).

The initiation of the first flower bud is delayed in *irp5-1, irp5-2, irp7-1 +/−, irp8-1 +/−, irp9-1 +/−, irp9-2 +/−* and *irp9-3 +/−* (Figure 4B, 5.1). In contrast, for most of the mutant lines (*irp1-1, irp2-1 +/−, irp2-2 +/−, irp5-1, irp5-2, irp6-1, irp7-1, irp8-1 +/−*) a faster flowering was observed (Figure 4B, 6.9). Standing out, *irp9-1 +/−, irp9-2 +/−* and *irp9-3 +/−* plants were delayed in general (Figure 4B, 1.02–6.9).

Thus, we observed four developmental phenotypes for the different factors. (I) The mutants of *IRP2* and *IRP3* showed a delayed initial growth. (II) The mutants of *IRP5*,
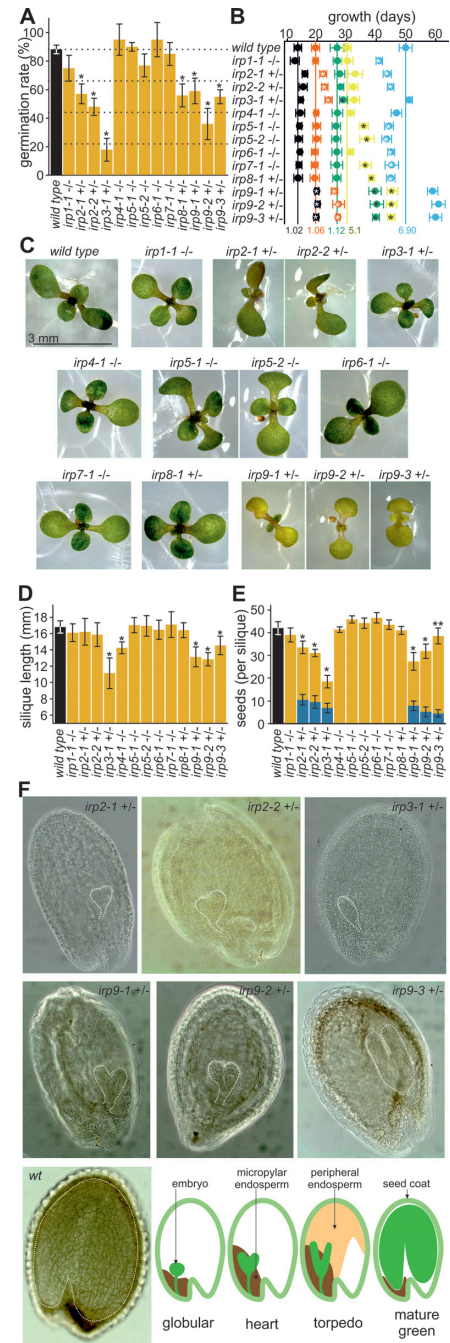

Figure 4. Growth and development of the mutants with defects in rRNA processing. (**A**) Germination rate for the different mutant lines was determined. Values with statistically significant difference to wild-type ($P < 0.001$) are indicated (*). (**B**) Growth analysis of the mutant lines according to Boyes *et al.* (62). The stage 1.02 (2 rosette leaves > 1 mm in length), 1.06 (6 rosette leaves >1 mm in length), 1.12 (12 rosette leaves >1 mm in length), 5.1 (first flower buds visible) and 6.9 (flowering complete) is shown. Values with statistically significant difference to wild-type ($P < 0.01$) are indicated (*). (**C**) A representative plant of the indicated mutants after 14 days of growth. (**D**, **E**) Silique length (D) and the number of seeds per silique (E) of the indicated mutants is presented. The black bar shows wild-type and the blue inset in (E) the number of pale seeds. Values with statistically significant difference to wild-type ($P < 0.001$, * or $P < 0.01$, **) are indicated. (**F**) Shown are representative pale seeds of the indicated six mutant strains. A green wild-type seed is shown for comparison. On the bottom there are illustrations of the globular, heart, linear cotyledon and mature green stage of the seeds. The illustrations are according to (77).

IRP7 and *IRP8* had a delay of initial flowering. (III) The mutants of all *IRP*s except *IRP3*, *IPR4* and *IRP9* showed an early completion of flowering, while (IV) the mutants of *IRP9* showed a general delay of growth. Remarkably, for *irp4-1* we observed only a weak developmental phenotype represented by extended inflorescence (Supplemental Figure S4).

Mutants of *IRP2*, *IRP3* and *IRP9* lead to an arrest of embryo development

We were unable to isolate homozygous mutants of *IRP2, IRP3, IRP8* and *IRP9*. Germination of the seeds of the according mutants shows an at least 25% reduction (Figure 4A). In addition, we observed a reduction in the length of the mature siliques for the mutants of *IRP3* and *IRP9* (as well as of *IRP4*) in comparison to wild-type (Figure 4D; Supplemental Figure S5). The number of seeds per silique is lower in the mutants of *IRP2, IRP3* and *IRP9* when compared to wild-type (Figure 4E). Moreover, we observed a significant number of pale seeds in the siliques of *IRP2, IRP3* and *IRP9*, but not of *IRP8* (Supplemental Figure S5).

Inspection of the pale seeds of *irp2-1* +/− and *irp2-2* +/− revealed that the embryo was arrested in the heart stage (Figure 4F; (78)). The embryo in pale seeds of *irp3-1* +/− was arrested in pro-embryo/globular stage (Figure 4F). For the mutants of *IRP9* the number of detected pale seeds was lower than for *IRP2* and *IRP3*. Moreover, the three *IRP9* mutants showed a somewhat differential phenotype likely caused by the different T-DNA insertion site. While embryos in pale seeds of *irp9-1* +/− and *irp9-2* +/− were mostly arrested in the heart stage, most of the pale seeds of *irp9-3* +/− contained embryos in the torpedo stage (Figure 4F). Thus, the pale seeds observed in the siliques of *IRP2, IRP3* and *IRP9* explain the lower germination rate of the according mutants.

The stage of embryo developmental arrest parallels the previously established expression profile (Supplemental Figure S2; (76,77)), where IRP2 was found to be highly expressed in preglobular, globular and heart stage, IRP3 transcript abundance increases from preglobular to globular stage and IRP9 transcript is high in the preglobular and the heart stage. Moreover, the observed phenotype of arrested embryo development in pale seeds is comparable to that found for mutants of other RBFs (29).

IRP5, IRP6 and IRP7 function is required during auxin induced growth

It has been proposed that ribosome biogenesis is regulated by the phytohormone auxin (31,37–39). In turn, auxin induces cell growth and division which requires high rates of protein synthesis and defects in ribosome biogenesis would cause alterations of the plant response to auxin. This is documented by an enhanced activity of e.g. RNA polymerase I required for rRNA precursor synthesis (79–81). Hence, auxin treatment will highlight the importance of ribosome biogenesis factors for maturation of the early rRNA precursors. Consequently, we analyzed the rRNA processing of the homozygotes *IRP5, IRP6* and *IRP7* mutants showing

an enhanced level particularly of 33S and 27S pre-rRNA (Figure 3) after treatment with 10 μM auxin (Figure 5A; (82)) to define the time of action of the according factors.

For wild-type we observed that auxin treatment reduced the abundance of the early forms of pre-rRNA (35S, 33S, $27SA_2/A_3$ and $27SB_{S/L}$), while the late forms of pre-rRNAs are not as drastically affected in their abundance (P-A_3, P'-A_3 or 18S-A_3; Figure 5A, B left). For *irp5-1* we detected a further increase of the accumulation of 33S after auxin treatment when compared to untreated plants (Figure 5B). Thus, in comparison to wild-type where 33S abundance is reduced upon auxin treatment, the observed pre-rRNA processing phenotype (Figure 3) is even more pronounced.

Auxin treatment of *irp6-1* yielded an increase of the 35S as well as of $27SB_{S/L}$ pre-rRNA when compared to wild-type and the untreated mutant (Figure 5A, B). The $27SA_2/A_3$ remained enhanced in the mutant, but did not show a further accumulation when compared to untreated wild-type (Figure 5A, B). For *irp7-1* we realized an accumulation of P-A_3 and P'-A_3 intermediates when compared to the plants grown in the absence of auxin (Figure 5A, B). Moreover, we observed the accumulation of an additional rRNA intermediate with probe p2 (Figure 5A, triangle).

Inspired by the observed additional rRNA intermediate after auxin treatment of the *irp7-1* mutant we compared the profile of pre-rRNAs isolated from flowers and cell cultures representing a fast dividing system. While the additional intermediate was barely detectable in flowers, it is present in the cell culture (Figure 5C, star). Circular RT-PCR and sequencing of the fragment revealed that the 5′ end originates from cleavage at P-site and the 3′ end from cleavage at C_2 and subsequent endo- or exonuclease activity (Figure 5D). Remarkably, while sequencing the intermediates we realized few fragments with poly-A adenylation consistent with tagging for degradation (83).

The *irp* mutants are sensitive to salt and sugar stress

Ribosome biogenesis was linked to stress responses and sugar provision (27,32,33). Consequently, we analyzed the growth of the *irp* mutants in the presence of 100mM NaCl (Figure 6A). We realized a reduced growth of all mutants judged from the rosette diameter when compared to wild-type. The strongest reduction is observed for *irp2-1, irp2-2, irp3-1, irp9-1, irp9-2* and *irp9-3* (Figure 6A, classes d, cd and c). Moreover, all mutants except *irp4-1*, *irp7-1* and *irp8-1* show a chlorotic phenotype. In contrast, the wild-type is just slightly impaired in growth when compared to normal growth conditions and does not show chlorosis.

Growth on 200 mM glucose showed a different phenotypic pattern. Here, *irp4-1, irp6-1* and *irp7-1* show no significant reduction of growth when compared to wild-type (Figure 6B, class ab). All other T-DNA insertion lines show reduced growth and an enhanced anthocyanin level which has been associated with sugar stress (27,84). Nevertheless, *irp2-1, irp2-2, irp5-1*, *irp8-1, irp9-1, irp9-2* and *irp9-3* showed a more dramatic effect than the other three mutant lines (Figure 6B, classes d, cd, c). Thus, we are able to link the function of IRPs to abiotic stress response, but at the same time realized that not all IRPs are equally important.
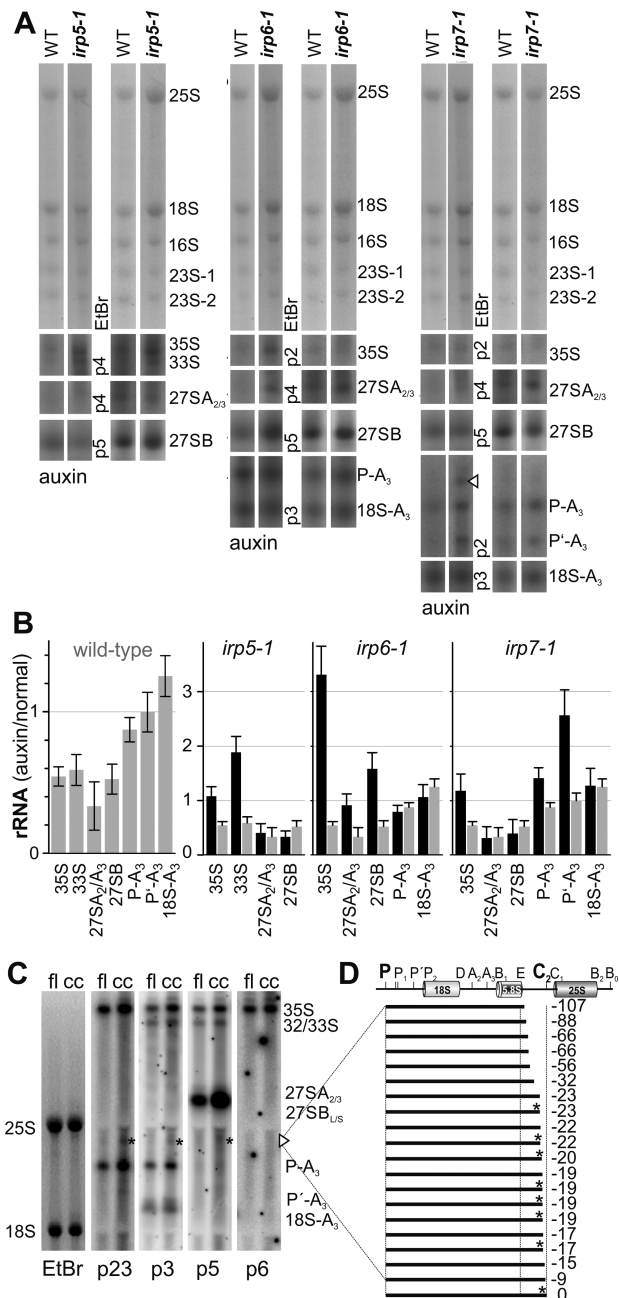
Figure 5. rRNA processing after auxin treatment. (**A**) Representative northern blots with probes indicated on the left for *irp5-1, irp6-1* and *irp7-1* grown in the presence of or absence of 0.5 mM auxin is shown. The name of the rRNA intermediate is indicated on the right. (**B**) Quantification of the intensities of the northern blot results for the different rRNA intermediates shown in (A). Values were normalized to the ethidium bromide stained mature 25S and 18S and are expressed as ratio between signal after auxin treatment and without auxin treatment. Black bars show values for T-DNA insertion lines and grey bars for wild-type. Standard deviation is shown. (**C**) Representative northern blots, with probes indicated (bottom), using isolated RNA from flowers (fl) and cell cultures (cc). The annealing of the probes is indicated in Figure 3A. The migration of the mature rRNA is indicated on the left and of the rRNA intermediates are indicated on the right. The triangle marks the new P-C_2 intermediates, which is highlighted by a star and not detectable with p6. (**D**) The fragments were mapped to rRNA for determining the extremities with respect to P and C_2 site (n = 21) and the number (right) the distance from C_2. Star indicates fragments with polyadenylation.

DISCUSSION

Additional nine factors influencing rRNA processing in *A. thaliana*

We have identified nine proteins without yeast or human RBF orthologue (Figure 1; Table 2) that play an important role in rRNA processing in *A. thaliana* (Figure 3). We annotated the factors and the according mutants as 'involved in rRNA processing' (IRP). Thus, we provide evidence of plant-specific RBFs which are involved in the processing of various plant pre-rRNA precursors, ranging from 33S maturation to processing of the 5′-5.8S pre-rRNA.

Mutants of *IRP1* to *IRP4* show a reduction of the 35S pre-rRNA (Figures 3 and 7). In addition, the 33S pre-rRNA is reduced in the mutants of *IRP2* to *IRP4* and the 27S-$B_{S/L}$ pre-rRNA in the mutant of *IRP3*. This links the function of IRP1, IRP2 and IRP3 to the transcription of 35S or to the regulation of 35S or 33S stability.

In addition to the impact on larger pre-rRNAs, the mutation of IRP4 causes an enhanced occurrence of the 5.8S+30 and 6S pre-rRNA (Figure 3). This suggests that IRP4 is involved in the final maturation of the 3′ end of the 5.8S rRNA and that accumulation of the larger pre-rRNAs might be a feed back to the delay of 5.8S processing.

The mutant of *IRP5* causes an accumulation of the 33S pre-rRNA (Figures 3 and 5) and the mutant of *IRP6* defective in 27S-$B_{S/L}$ cleavage (Figures 3 and 5). Thus, IRP5 and IRP6 are likely involved in the early rRNA maturation. Again, the accumulation of 27S-$A_{2/3}$ in the mutant of *IRP6* might be the consequence of the delay in 27S-$B_{S/L}$ pre-rRNA processing.

IRP7 appears to be involved in processing of P'-A_3 (Figure 3) and its mutation causes the accumulation of a P-C_2 pre-rRNA upon addition of auxin (Figure 5). Mutation of IRP8 causes an accumulation of the 18S-A_3 pre-rRNA. Thus, the function of these two IRPs affects the maturation of the small subunit. Worthwhile mentioning, the mutant of IRP8 shows an accumulation of other pre-rRNAs as well (Figure 3).

Moreover, IRP7, IRP8 and IRP9 affect the processing of the plant-specific rRNA intermediate 5′-5.8S (Figures 3 and 7). Thus, four of the identified proteins are involved in plant-specific rRNA processing pathways (5′-5.8S and P-C_2 pre-rRNA cleavage).

The IRPs are largely conserved in plants

IRP2, IRP4 and IRP9 are conserved in all eukaryotes (Figure 1, Table 2), but their orthologues in yeast or humans have no described function as RBF. All three proteins have been annotated in the past, but only for IRP2 and IRP4 an additional function has been identified. This is not unexpected because several human disease-related genes (e.g. DUSP11 or NOL7), and likewise the yeast proteins Snu66, a component of the spliceosome and the pre-mRNA splicing factor Prp43p were described to be involved in rRNA processing (23,85,86). Based on the overlap between proteome analysis after fractionation (24) and intracellular distribution of GFP-fusion proteins IRP2, IRP4 and IRP9 are localized in the nucleus (Figure 2).
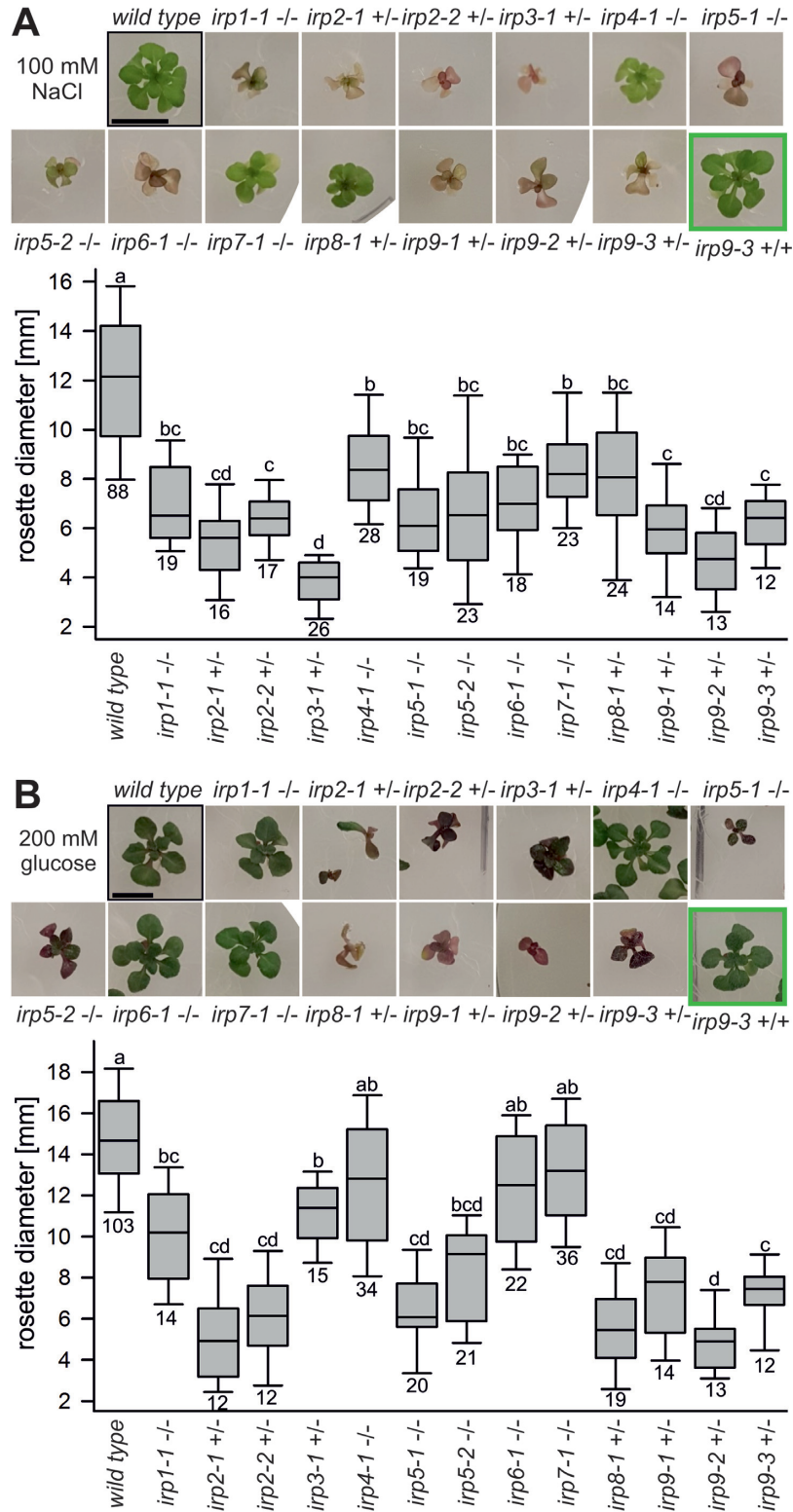
Figure 6. Sensitivity of *irp* mutants to salt and glucose. (**A, B**) Representative images of plants grown on plates supplemented with 100 mM NaCl (A) or 200 mM glucose (B) are shown on the top. The diameter of the plants was determined and the results for the indicated number of plants (number below box) is shown as a box plot. For heterozygous lines the diameter was first clustered and after occurrence of two populations the one with diameters like wild-type was omitted. Significance of the differences was analyzed ($P < 0.001$) and same letters indicate values without statistically significant variation.

Table 2. Properties of T-DNA insertion lines affecting rRNA processing

TG	OG	Occurrence	Line name	Stock center ID	Zygosity	DD	Salt sensitivity	Sugar sensitivity
AT3G07170		Streptophyta	irp1-1	Salk_006113.53.35.x	Homozygote	Early flowering	C/RRD[C]	RRD[C]
AT4G32720		Eukaryota	irp2-1	Sail_313C08	Heterozygote	Arrested embryo dev.	C/RRD	A/RRD
			irp2-2	Gabi_870F12	Heterozygote	Arrested embryo dev.	C/RRD	A/RRD
AT4G17720	AT5G16840	Viridiplantae	irp3-1	Sail_365B01	Heterozygote	Arrested embryo dev.	C/RRD	A/RRD
AT3G11270	AT5G05780	Eukaryota	irp4-1	Salk_128568.33.50.x	Homozygote	Reduction of silique length	RRD	-
AT1G29250	AT2G34160	Viridiplantae	irp5-1	Gabi_560B06	Homozygote	Growth delay, early flowering	C/RRD	A/RRD
			irp5-2	Salk_069210.55.50.x	Homozygote	Growth delay, early flowering	C/RRD	A/RRD
AT3G01540	AT3G06480 AT5G14610	Streptophyta[A,B]	irp6-1	Salk_073018.54.25.x	Homozygote	Early flowering	C/RRD	-
AT2G34160	AT1G29260	Viridiplantae	ipr7-1	Gabi_128D08	Homozygote	Growth delay, early flowering	RRD	-
AT1G66260	AT5G37720	Magnoliophyta	ipr8-1	Gabi_714H09	Heterozygote	Reduced germination growth delay, early flowering	RRD	A/RRD
			irp9-1	Salk_077667.14.70.n	Heterozygote	Arrested embryo dev., growth delay	C/RRD	A/RRD
AT4G25550		Eukaryota	irp9-2	Salk_032994.56.00.x	Heterozygote	Arrested embryo dev., growth delay	C/RRD	A/RRD
			irp9-3	Salk_117288.49.45.x	Heterozygote	Arrested embryo dev. growth delay	C/RRD	A/RRD

TG…targeted gene; OG…orthologous genes; DD…developmental defects, RSS…response to salt or sugar stress; A: orthologues identified in few archaeal genomes, B: orthologues identified in few bacterial genomes; C: chlorotic (C) phenotype, enhanced anthocyanin content (A) or reduced rosette dimension (RRD).

IRP2 contains a RRM and a La domain that are known to bind RNA (Figure 1; (67,68)). The protein was identified as a homologue of the human La1 protein and an embryonic-lethal phenotype was reported (87), which is consistent with our observation (Figure 4; Supplemental Figure S5). It was reported that AtLa1/IRP2 binds to the 5′UTR of the WUS mRNA (88) and interacts with pre-snoR43.1 (87) targeting the 18S rRNA (89). Considering the impact on snoRNA production, we cannot exclude that the impact of AtLa1/IRP2 on rRNA processing is indirect through snoR43.1 maturation.

IRP4 was previously assigned as subunit Rpn8b of the 26S proteasome (72). We conclude that the impact of Rpn8p/IRP4 on ribosome biogenesis might be linked to a defect of the 26S proteasome, especially as subunits of the 26S proteasome have been identified in the nucleolus as well (47). Moreover, AT5G05780 not analyzed here is orthologous to IRP4. Consistent with the existence of an orthologue with similar function, we were able to isolate a homozygote mutant that shows only a weak phenotype (Figure 4; Supplemental Figure S1).

IRP9 contains a domain annotated as nucleotide hydrolase and was annotated as cleavage factor CFIS2 of the polyadenylation machinery (74). However, despite a yeast two hybrid analysis yielding an interaction with the endonuclease CPSF30, the poly(A) tail binding protein PAPS4 and a fragment of the PAPS binding partner FIPS5 (74), the function in plants was not yet demonstrated. Remarkably, the heterozygous mutant shows a significant growth reduction (Figure 4; Supplemental Figure S4) and an accumulation of the 5′-5.8S pre-rRNA (Figure 3).

Among the factors with impact on rRNA processing, IRP3, IRP5, IRP7 and IRP8 are found in all Viridiplantae (Figure 1). IRP3 contains an RRM domain (Figure 1) and is at least localized in the cytosol and nucleus (Figure 2). The mutant is embryonic-lethal (Figure 4). This suggests that the observed orthologue (AT5G16840; Table 2) does not perform a comparable function. The heterozygous mutant of *IRP3* showed defects in accumulation of 35S, 33S and 27S-$B_{S/L}$ pre-rRNA (Figure 3). The nucleolar localized IRP8 is characterized by an RRM domain and was previously annotated as ALY3 without further experimental analysis (Figure 2; (90)). The defect of rRNA processing is widespread (Figures 3 and 7). Remarkably, IRP8 contains a PRMT1 domain, which is characteristic for methyltransferases (Figure 1). Recently, a comparable widespread impact on rRNA maturation was described for the methyltransferase AtPRMT3 (91). Considering that IRP8 contains an RRM domain for RNA interaction, the widespread function of IRP8 is consistent with a global function in rRNA processing in plants as assigned to AtPRMT3.

IRP5 and IRP7 are orthologues, but perform different functions. The proteins contain an ALBA domain (66). By GFP-fusion we identified IRP5 in the cytosol and IRP7 in the cytosol and nucleus (Figure 2, Table 1), and by mass spectrometry in the nucleolus (24). Considering the impact of IRP5 on 33S processing and of IRP7 on P'-A_3 processing (Figures 3 and 5) it is likely that the GFP-fusion resulted in mistargeting of the protein. The mutant of *IRP5* and *IRP7* showed a delay of initial flowering and a reduced inflorescence stem growth (Figure 4, Supplemental Figure S4).

Two proteins are specific for Streptophyta, namely IRP1 and IRP6 (Figure 1). IRP1 is localized in the nucleus and

nucleolus (Figure 2) and contains a SAM-domain (Figure 1; (70,71)). The protein is not essential (Supplemental Figure S1) and the mutant shows a reduced accumulation of the 35S rRNA (Figure 3). IRP6 belongs to the DEAD/DEAH-helicases and was annotated as atDRH1 (92). A recent study suggested a function of atDRH1/IRP6 in the regulation of mRNA export from the nucleus based on the mRNA accumulation in the mutants (93). In agreement with this notion, the GFP-fusion protein was localized in nucleoplasm and cytoplasm (Figure 2). However, the protein is also present in the nucleolus (Figure 2, (24)) and especially 27S-A$_{2/3}$ pre-rRNAs accumulate in the mutant (Figure 3).

Thus, we identified six proteins that are either plant-specific or have plant-specific functions as RBF (IRP2, IRP3, IRP4, IRP7, IRP8 and IRP9). However, two of the analyzed IRPs (IRP2 and IRP4) might function upstream of processes directly involved in rRNA maturation. Nevertheless, their function is central for rRNA processing as the abundance of specific pre-rRNAs is affected in the according mutants. In addition, two IRPs are specific for Streptophyta (IRP1 and IRP6).

The link between rRNA processing and cell physiology

The importance of ribosome biogenesis is already reflected by the circumstance that homozygous mutants of four of the nine IRPs are lethal, while mutants of two of the other four factors (IRP5 and IRP7) show a reduced growth (Figure 4). Here, *IRP2* mutants, *irp3-1* and *IRP9* mutants show an embryo development phenotype (Figure 4, Supplemental Figure S5). The *irp8-1* line does not show a reduced seed number but a reduced germination rate by 25%. This suggests that the mutant is recessive lethal allowing development of the embryo but impeding germination. This explains the absence of mature homozygous mutant plants (Figure 4). The survival of the embryo not expressing a functional variant of a given IRP to a certain state might be explained by the function of pre-existing proteins that is constantly diluted by cell division to a level no longer sufficient to promote proper ribosome maturation. Our results further document that the orthologue of IRP3 encoded by *AT5G16840* (Table 2) and the orthologue of IRP8 encoded by *AT5G37720* (Table 2) do not perform the same function.

The heterozygous mutants of *IRP2* and *IRP9* were delayed in growth when compared to wild-type (Figure 4; Supplemental Figure S4). In addition, the mutants of *IRP1, IRP2, IRP5, IRP6* and *IRP7* show an early flowering, which is a typical stress characteristic (94). Such drastic phenotype is in agreement with previous reports for plant RBFs (27,29,36,42–45) and documents the importance of ribosome biogenesis for cell survival.

The mutants of *IRP1, IRP4* and *IRP6* show only a weak phenotype under normal growth conditions (Figure 4, Supplemental Figure S4). For IRP4 and IRP6 this might in part be explained by the existence of orthologues AT5G05780 for IRP4 and AT3G06480 for IRP6, which could perform a comparable function (Table 2). Interestingly, the mutant of the orthologue of IRP6 encoded by *AT5G14610* did not show any defects in pre-rRNA maturation (Figure 3). In turn, the mutant of *IRP6* like the mutant of *IRP5* showed a more pronounced defect in pre-rRNA processing after enforcing growth by addition of auxin (Figure 5). It is well established that auxin treatment enhances pre-rRNA synthesis (79–81). This might suggest that the function of IRP6 becomes rate limiting under conditions with pre-rRNA synthesis and that the additional factors with comparable function are not fully sufficient under this condition (Figures 3 and 7).

It has been reported that sugar deprivation leads to reduced rRNA synthesis (33), while sugar treatment enhances the expression of RBF and RP genes as well as genes coding for subunits of snoRNP complexes (34). This is consistent with the observed high sugar content in meristem tissues with high rates of cell divisions and thus, a high demand on energy (95). Mutants of the RBFs APUM24 or AtRH57 show hyper sensitivity to high sugar contents (27,96), similar to the phenotype of the mutants of *IRP2, IRP5, IRP8* and *IRP9* (Figure 6). Based on the analysis of mutants of AtRH57 it was proposed that RBFs might act in feedback inhibition of glucose induced abscisic acid accumulation (97), the latter causing a delay of germination, growth and assembly of photosystems (97). Thus, the process of ribosome maturation is directly linked to the cellular fate in cells with high energy supply.

Remarkably, the mutants of the other *IRP*s (IRP1, IRP4, IRP6, IRP7) are not as drastically affected by addition of glucose. Note, all four are not essential in general and for three we even observed orthologous sequences (Table 1). In turn, all mutants are highly sensitive to salt stress when compared to wild-type and most even show chlorosis (Figure 6). In general, high salinity represents an abiotic stress that causes ionic toxicity and osmotic changes (98). In response, a reprogramming of the cellular proteome occurs that requires massive protein synthesis (99). Thus, ribosome biogenesis is required to cope with the new cellular situation and accordingly, mutants with reduced synthesis rates exhibit a loss of response capacity. Indeed, this is consistent with the previous suggestion that the fidelity of ribosome biogenesis under salt stress is regulated by post-translational processing and might even involve abscisic acid signaling (32). The latter would unify the responses of ribosome biogenesis to the energy supply and to stress responses, at least to salt stress responses, which needs to be explored in more detail in future.

The plant-specific pre-rRNA processing events

We discovered three IRPs involved in the maturation of the plant-specific 5′-5.8S pre-rRNA (Figure 3) and discovered an ITS2 cleavage first mode in fast dividing tissues (Figure 5). While IRP7 and IRP8 influence the maturation of the small ribosomal subunit as well, IRP9 appears to be exclusively involved in 5′-5.8S pre-rRNA maturation (Figure 3). Remarkably, mutants of *IRP9* involved in the processing of the plant-specific precursor 5′-5.8S (2) showed the strongest phenotype, as the mutation caused embryo lethality, and even the heterozygous mutants showed reduced growth and a pale-leaf phenotype in the early phase. In addition, *IRP9* mutants were highly sensitive to high salt and sugar treatment. This demonstrates that processing of the plant-specific 5′-5.8S precursor is essential for viability,
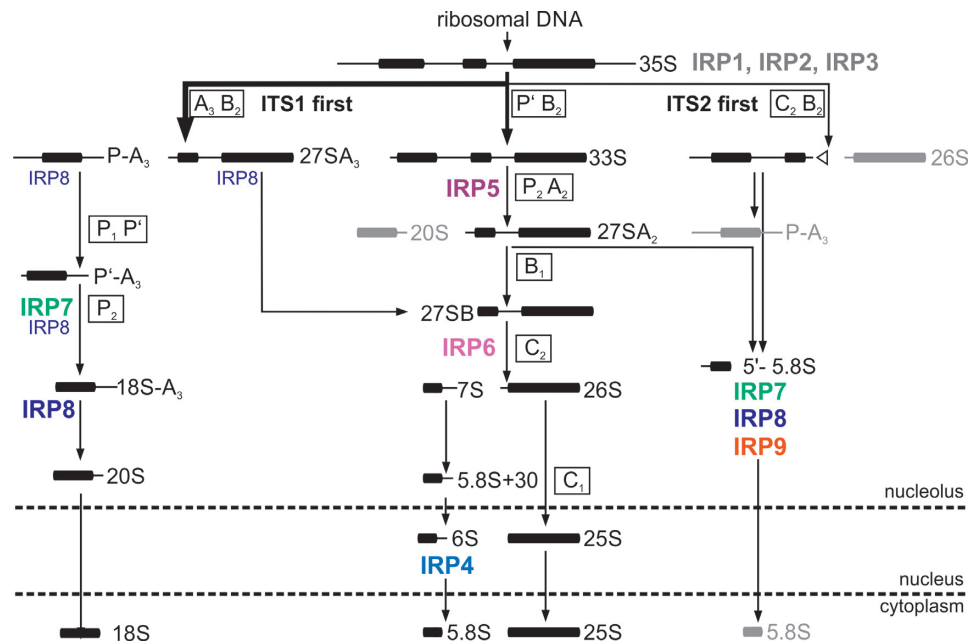
Figure 7. The impact of the IRPs in rRNA processing. The rRNA processing scheme in plants according to (2) with modifications to include our observations is shown. The arrow size on top illustrates the general importance of the major (ITS1 first), the minor (5′ETS first) and the 'bypass' (ITS2 first) pre-rRNA maturation pathway. The involvement of the IRPs in pre-rRNA processing according to Figures 3 and 5 are shown. The color of the IRP name is a simple guidance for the involvement in different pathways. Note, the effect of IRP8 is dispersed. Intermediates in grey are further processed according to the pathways shown before on the left side.

while the 6S pre-rRNA exists in parallel (2), and that IRP9 appears to be central for this processing. The exact mechanism by which IRP9 regulates the processing remains to be established. In turn, the mutant of *IRP4* which is involved in the maturation of 6S pre-rRNA is not lethal and does not show a strong phenotype. Whether this reflects a lower demand for 6S processing than for 5′-5.8S pre-rRNA maturation or whether the orthologue can perform the same function, especially as both are expressed in comparable manner e.g. in seeds (Supplemental Figure S4) needs to be further investigated.

Moreover, an additional pre-rRNA intermediate became detectable in *irp7-1* after enforced growth by auxin addition (Figure 5). As mentioned above, addition of auxin on the one hand enforces cell growth and division and on the other hand accelerates pre-rRNA synthesis. Thus, in normal tissues the absence of IRP7 is not rate limiting, while enhancing pre-rRNA synthesis uncovers the importance of the factor. However, this intermediate becomes detectable in fast dividing tissues represented in here by cell cultures (Figure 5). The intermediate represents a pre-rRNA produced by P and C_2 cleavage and thus represents an ITS2 cleavage first pathway (Figure 7) not yet identified in yeast or humans. Thus, we have three pathways of pre-rRNA maturation in plants, the previously described (i) ITS1 cleavage first and (ii) the 5′-ETS removal first (2), as well as the in here identified ITS2 cleavage first (Figure 7). Based on current knowledge we assume that the latter represents a pathway occurring in fast dividing tissues. The importance of the third pre-rRNA maturation pathway needs to be explored in the future.

SUPPLEMENTARY DATA

Supplementary Data are available at NAR Online.

REFERENCES

1. Kressler,D., Hurt,E. and Baßler,J. (2017) A puzzle of life: crafting ribosomal subunits. *Trends Biochem. Sci.*, **42**, 640–654.
2. Weis,B.L., Kovacevic,J., Missbach,S. and Schleiff,E. (2015) Plant-specific features of ribosome biogenesis. *Trends Plant Sci.*, **20**, 729–740.

3. Henras,A. K., Soudet,J., Gerus,M., Lebaron,S., Caizergues-Ferrer,M., Mougin,A. and Henry,Y. (2008) The post-transcriptional steps of eukaryotic ribosome biogenesis. *Cell Mol. Life Sci.*, **65**, 2334–2359.

4. Konikkat,S. and Woolford,J.L. Jr (2017) Principles of 60S ribosomal subunit assembly emerging from recent studies in yeast. *Biochem. J.*, **474**, 195–214.

5. Sloan,K.E., Warda,A.S., Sharma,S., Entian,K.D., Lafontaine,D.L.J. and Bohnsack,M.T. (2017) Tuning the ribosome: The influence of rRNA modification on eukaryotic ribosome biogenesis and function. *RNA Biol.*, **14**, 1138–1152.

6. Lafontaine,D.L. (2015) Noncoding RNAs in eukaryotic ribosome biogenesis and function. *Nat. Struct. Mol. Biol.*, **22**, 11–19.

7. Burlacu,E., Lackmann,F., Aguilar,L.C., Belikov,S., Nues,R.V., Trahan,C., Hector,R.D., Dominelli-Whiteley,N., Cockroft,S.L., Wieslander,L. *et al.* (2017) High-throughput RNA structure probing reveals critical folding events during early 60S ribosome assembly in yeast. *Nat. Commun.*, **8**, 714.

8. Cheng,J., Kellner,N., Berninghausen,O., Hurt,E. and Beckmann,R. (2017) 3.2-Å-resolution structure of the 90S preribosome before A1 pre-rRNA cleavage. *Nat. Struct. Mol. Biol.*, **24**, 954–964.

9. Chaker-Margot,M., Barandun,J., Hunziker,M. and Klinge,S. (2017) Architecture of the yeast small subunit processome. *Science*, **355**, eaal1880.

10. Greber,B.J., Gerhardy,S., Leitner,A., Leibundgut,M., Salem,M., Boehringer,D., Leulliot,N., Aebersold,R., Panse,V.G. and Ban,N. (2016) Insertion of the biogenesis factor Rei1 probes the ribosomal tunnel during 60S maturation. *Cell*, **164**, 91–102.

11. Heuer,A., Thomson,E., Schmidt,C., Berninghausen,O., Becker,T., Hurt,E. and Beckmann,R. (2017) Cryo-EM structure of a late pre-40S ribosomal subunit from *Saccharomyces cerevisiae*. *Elife*, **6**, e30189.

12. Johnson,M.C., Ghalei,H., Doxtader,K.A., Karbstein,K. and Stroupe,M.E. (2017) Structural heterogeneity in pre-40S ribosomes. *Structure*, **25**, 329–340.

13. Kornprobst,M., Turk,M., Kellner,N., Cheng,J., Flemming,D., Koš-Braun,I., Koš,M., Thoms,M., Berninghausen,O., Beckmann,R. *et al.* (2016) Architecture of the 90S pre-ribosome: A structural view on the birth of the eukaryotic ribosome. *Cell*, **166**, 380–393.

14. Sarkar,A., Thoms,M., Barrio-Garcia,C., Thomson,E., Flemming,D., Beckmann,R. and Hurt,E. (2017) Preribosomes escaping from the nucleus are caught during translation by cytoplasmic quality control. *Nat. Struct. Mol. Biol.*, **24**, 1107–1115.

15. Scaiola,A., Peña,C., Weisser,M., Böhringer,D., Leibundgut,M., Klingauf-Nerurkar,P., Gerhardy,S., Panse,V.G. and Ban,N. (2018) Structure of a eukaryotic cytoplasmic pre-40S ribosomal subunit. *EMBO J.*, **37**, e98499.

16. Schuller,J.M., Falk,S., Fromm,L., Hurt,E. and Conti,E. (2018) Structure of the nuclear exosome captured on a maturing preribosome. *Science*, **360**, 219–222.

17. Yip,W.S., Vincent,N.G. and Baserga,S.J. (2013) Ribonucleoproteins in archaeal pre-rRNA processing and modification. *Archaea*, **2013**, 614735.

18. Ebersberger,I., Simm,S., Leisegang,M.S., Schmitzberger,P., Mirus,O., von Haeseler,A., Bohnsack,M.T. and Schleiff,E. (2014) The evolution of the ribosome biogenesis pathway from a yeast perspective. *Nucleic. Acids. Res.*, **42**, 1509–1523.

19. Simm,S., Fragkostefanakis,S., Paul,P., Keller,M., Einloft,J., Scharf,K.D. and Schleiff,E. (2015) Identification and expression analysis of ribosome biogenesis factor co-orthologs in *Solanum lycopersicum*. *Bioinform. Biol. Insights*, **9**, 1–17.

20. Larburu,N., Montellese,C., O'Donohue,M.F., Kutay,U., Gleizes,P.E. and Plisson-Chastang,C. (2016) Structure of a human pre-40S particle points to a role for RACK1 in the final steps of 18S rRNA processing. *Nucleic Acids Res.*, **44**, 8465–8478.

21. Simabuco,F.M., Morello,L.G., Aragão,A.Z., Paes Leme,A.F. and Zanchin,N.I. (2012) Proteomic characterization of the human FTSJ3 preribosomal complexes. *J. Proteome Res.*, **11**, 3112–3126.

22. Sloan,K.E., Bohnsack,M.T., Schneider,C. and Watkins,N.J. (2014) The roles of SSU processome components and surveillance factors in the initial processing of human ribosomal RNA. *RNA*, **20**, 540–550.

23. Taffoureau,L., Zorbas,C., Langhendris,J.L., Mullineux,S.T., Stamatopoulou,V., Mullier,R., Wacheul,L. and Lafontaine,D.L. (2013) The complexity of human ribosome biogenesis revealed by systematic nucleolar screening of pre-rRNA processing factors. *Mol. Cell*, **51**, 539–551.

24. Palm,D., Simm,S., Darm,K., Weis,B.L., Ruprecht,M., Schleiff,E. and Scharf,C. (2016) Proteome distribution between nucleoplasm and nucleolus and its relation to ribosome biogenesis in *Arabidopsis thaliana*. *RNA Biol*, **13**, 441–454.

25. Mills,E.W. and Green,R. (2017) Ribosomopathies: There's strength in numbers. *Science*, **358**, eaan2755.

26. Neelamraju,Y., Hashemikhabir,S. and Janga,S.C. (2015) The human RBPome: from genes and proteins to human disease. *J. Proteomics*, **127**, 61–70.

27. Maekawa,S., Ishida,T. and Yanagisawa,S. (2018) Reduced expression of APUM24, encoding a novel rRNA processing factor, induces sugar-dependent nucleolar stress and altered sugar responses in *Arabidopsis thaliana*. *Plant Cell*, **30**, 209–227.

28. Nicolas,E., Parisot,P., Pinto-Monteiro,C., de Walque,R., De Vleeschouwer,C. and Lafontaine,D.L. (2016) Involvement of human ribosomal proteins in nucleolar structure and p53-dependent nucleolar stress. *Nat. Commun.*, **7**, 11390.

29. Missbach,S., Weis,B.L., Martin,R., Simm,S., Bohnsack,M.T. and Schleiff,E. (2013) 40S ribosome biogenesis co-factors are essential for gametophyte and embryo development. *PLoS One*, **8**, e54084.

30. Zakrzewska-Placzek,M., Souret,F.F., Sobczyk,G.J., Green,P.J. and Kufel,J. (2010) Arabidopsis thaliana XRN2 is required for primary cleavage in the pre-ribosomal RNA. *Nucleic Acids Res.*, **38**, 4487–4502.

31. Zhao,H., Lü,S., Li,R., Chen,T., Zhang,H., Cui,P., Ding,F., Liu,P., Wang,G., Xia,Y. *et al.* (2015) The Arabidopsis gene DIG6 encodes a large 60S subunit nuclear export GTPase 1 that is involved in ribosome biogenesis and affects multiple auxin-regulated development processes. *J. Exp. Bot.*, **66**, 6863–6875.

32. Huang,K.C., Lin,W.C. and Cheng,W.H. (2018) Salt hypersensitive mutant 9, a nucleolar APUM23 protein, is essential for salt sensitivity in association with the ABA signaling pathway in Arabidopsis. *BMC Plant Biol.*, **18**, 40.

33. Ishida,T., Maekawa,S. and Yanagisawa,S. (2016) The pre-rRNA processing complex in Arabidopsis includes two WD40-domain-containing proteins encoded by glucose-inducible genes and plant-specific proteins. *Mol. Plant*, **9**, 312–315.

34. Kojima,H., Suzuki,T., Kato,T., Enomoto,K., Sato,S., Kato,T., Tabata,S., Sáez-Vasquez,J., Echeverría,M., Nakagawa,T. *et al.* (2007) Sugar-inducible expression of the nucleolin-1 gene of *Arabidopsis thaliana* and its role in ribosome synthesis, growth and development. *Plant J.*, **49**, 1053–1063.

35. Kalinina,N.O., Makarova,S., Makhotenko,A., Love,A.J. and Taliansky,M. (2018) The multiple functions of the nucleolus in plant development, disease and stress responses. *Front. Plant Sci.*, **9**, 132.

36. Weis,B.L., Palm,D., Missbach,S., Bohnsack,M.T. and Schleiff,S. (2015) atBRX1-1 and atBRX1-2 are involved in an alternative rRNA processing pathway in Arabidopsis thaliana. *RNA*, **21**, 1–11.

37. Rosado,A., Sohn,E.J., Drakakaki,G., Pan,S., Swidergal,A., Xiong,Y., Kang,B.H., Bressan,R.A. and Raikhel,N.V. (2010) Auxin-mediated ribosomal biogenesis regulates vacuolar trafficking in *Arabidopsis*. *Plant Cell*, **22**, 143–158.

38. Huang,C.K., Shen,Y.L., Huang,L.F., Wu,S.J., Yeh,C.H. and Lu,C.A. (2016) The DEAD-Box RNA helicase AtRH7/PRH75 Participates in Pre-rRNA Processing, plant development and cold tolerance in *Arabidopsis*. *Plant Cell Physiol.*, **57**, 1741–1791.

39. Szakonyi,D. and Byrne,M.E. (2011) Ribosomal protein L27a is required for growth and patterning in Arabidopsis thaliana. *Plant J.*, **65**, 269–281.

40. Ahn,C.S., Cho,H.K., Lee,D.H., Sim,H.J., Kim,S.G. and Pai,H.S. (2016) Functional characterization of the ribosome biogenesis factors PES, BOP1, and WDR12 (PeBoW), and mechanisms of defective cell growth and proliferation caused by PeBoW deficiency in Arabidopsis. *J. Exp. Bot.*, **67**, 5217–5232.

41. Jeon,Y., Park,Y.J., Cho,H.K., Jung,H.J., Ahn,T.K., Kang,H. and Pai,H.S. (2015) The nucleolar GTPase nucleostemin-like 1 plays a role in plant growth and senescence by modulating ribosome biogenesis. *J. Exp. Bot.*, **66**, 6297–6310.

42. Weis,B.L., Missbach,S., Marzi,J., Bohnsack,M.T. and Schleiff,E. (2014) The 60S associated ribosome biogenesis factor LSG1-2 is required for 40S maturation in *Arabidopsis thaliana*. *Plant J.*, **80**, 1043–4056.

43. Kojima,K., Tamura,J., Chiba,H., Fukada,K., Tsukaya,H. and Horiguchi,G. (2018) Two nucleolar proteins, GDP1 and OLI2, function as ribosome biogenesis factors and are preferentially involved in promotion of leaf cell proliferation without strongly affecting leaf adaxial-abaxial patterning in *Arabidopsis thaliana*. *Front Plant Sci.*, **8**, 2240.

44. Abbasi,N., Kim,H.B., Park,N.I., Kim,H.S., Kim,Y.K., Park,Y.I. and Choi,S.B. (2010) APUM23, a nucleolar Puf domain protein, is involved in pre-ribosomal RNA processing and normal growth patterning in Arabidopsis. *Plant J.*, **64**, 960–976.

45. Shanmugam,T., Abbasi,N., Kim,H.S., Kim,H.B., Park,N.I., Park,G.T., Oh,S.A., Park,S.K., Muench,D.G., Choi,Y. *et al.* (2017) An Arabidopsis divergent pumilio protein, APUM24, is essential for embryogenesis and required for faithful pre-rRNA processing. *Plant J.*, **92**, 1092–1105.

46. Pendle,A.F., Clark,G.P., Boon,R., Lewandowska,D., Lam,Y.W., Andersen,J., Mann,M., Lamond,A.I., Brown,J.W. and Shaw,P.J. (2005) Proteomic analysis of the Arabidopsis nucleolus suggests novel nucleolar functions. *Mol. Biol. Cell.*, **16**, 260–269.

47. Montacié,C., Durut,N., Opsomer,A., Palm,D., Comella,P., Picart,C., Carpentier,M.C., Pontvianne,F., Carapito,C., Schleiff,E. *et al.* (2017) Nucleolar proteome analysis and proteasomal activity assays reveal a link between nucleolus and 26S Proteasome in A. thaliana. *Front. Plant Sci.*, **8**, 1815.

48. Li,L., Stoeckert,C.J. Jr and Roos,D.S. (2003) OrthoMCL: identification of ortholog groups for eukaryotic genomes. *Genome Res.*, **13**, 2178–2189.

49. Sonnhammer,E.L. and Östlund,G. (2015) InParanoid 8: orthology analysis between 273 proteomes, mostly eukaryotic. *Nucleic Acids Res.*, **43**, D234–D239.

50. Goodstein,D.M., Shu,S., Howson,R., Neupane,R., Hayes,R.D., Fazo,J., Mitros,T., Dirks,W., Hellsten,U., Putnam,N. *et al.* (2012) Phytozome: a comparative platform for green plant genomics. *Nucleic. Acids. Res.*, **40**, D1178–D1186.

51. Altenhoff,A.M., Glover,N.M., Train,C.M., Kaleb,K., Warwick Vesztrocy,A., Dylus,D., de Farias,T.M., Zile,K., Stevenson,C., Long,J. *et al.* (2018) The OMA orthology database in 2018: retrieving evolutionary relationships among all domains of life through richer web and programmatic interfaces. *Nucleic Acids Res.*, **46**, D477–D485.

52. Finn,R.D., Coggill,P., Eberhardt,R.Y., Eddy,S.R., Mistry,J., Mitchell,A.L., Potter,S.C., Punta,M., Qureshi,M., Sangrador-Vegas,A. *et al.* (2016) The Pfam protein families database: towards a more sustainable future. *Nucleic Acids Res.*, **44**, D279–D285.

53. Sigrist,C.J., de Castro,E., Cerutti,L., Cuche,B.A., Hulo,N., Bridge,A., Bougueleret,L. and Xenarios,I. (2013) New and continuing developments at PROSITE. *Nucleic. Acids. Res.*, **41**, D344–D347.

54. Finn,R.D., Clements,J. and Eddy,S.R. (2011) HMMER web server: interactive sequence similarity searching. *Nucleic Acids Res.*, **39**, W29–W37.

55. Schwacke,R., Schneider,A., van der Graaff,E., Fischer,K., Catoni,E., Desimone,M., Frommer,W.B., Flügge,U.I. and Kunze,R. (2003) ARAMEMNON, a novel database for Arabidopsis integral membrane proteins. *Plant Physiol.*, **131**, 16–26.

56. Huala,E., Dickerman,A.W., Garcia-Hernandez,M., Weems,D., Reiser,L., LaFond,F., Hanley,D., Kiphart,D., Zhuang,M., Huang,W. *et al.* (2001) The Arabidopsis Information Resource (TAIR): a comprehensive database and web-based information retrieval, analysis, and visualization system for a model plant. *Nucleic. Acids. Res.*, **29**, 102–105.

57. Sommer,M.S., Daum,B., Gross,L.E., Weis,B.L.M., Mirus,O., Abram,L., Maier,U.G., Kühlbrandt,W. and Schleiff,E. (2011) Chloroplast Omp85 proteins change orientation during evolution. *Proc. Natl. Acad. Sci. U.S.A.*, **108**, 13841–13846.

58. Edwards,K., Johnstone,C. and Thompson,C. (1991) A simple and rapid method for the preparation of plant genomic DNA for PCR analysis. *Nucleic Acids Res.*, **19**, 1349.

59. Thole,V., Alves,S.C., Worland,B., Bevan,M.W. and Vain,P. (2009) A protocol for efficiently retrieving and characterizing flanking sequence tags (FSTs) in *Brachypodium distachyon* T-DNA insertional mutants. *Nat. Protoc.*, **4**, 650–661.

60. Chomczynski,P. and Sacchi,N. (1987) Single-step method of RNA isolation by acid guanidinium thiocyanate-phenol-chloroform extraction. *Anal. Biochem.*, **162**, 156–159.

61. Sambrook,J. and Russell,D.W. (2001) *Molecular Cloning: A Laboratory Manual*. 3rd edn. Cold Spring Harbor Laboratory Press, NY.

62. Boyes,D.C., Zayed,A.M., Ascenzi,R., McCaskill,A.J., Hoffman,N.E., Davis,K.R. and Görlach,J. (2001) Growth stage-based phenotypic analysis of Arabidopsis: a model for high throughput functional genomics in plants. *Plant Cell*, **13**, 1499–1510.

63. Sprunck,S., Rademacher,S., Vogler,F., Gheyselinck,J., Grossniklaus,U. and Dresselhaus,T. (2012) Egg cell–secreted EC1 triggers sperm cell activation during double fertilization. *Science*, **338**, 1093–1097.

64. Hakimi,H., Suganuma,K., Usui,M., Masuda-Suganuma,H., Angeles,J.M., Asada,M., Kawai,S., Inoue,N. and Kawazu,S. (2014) *Plasmodiumknowlesi* thioredoxin peroxidase 1 binds to nucleic acids and has RNA chaperone activity. *Parasitol. Res.*, **113**, 3957–3962.

65. Ramakrishnan,V., Finch,J.T., Graziano,V., Lee,P.L. and Sweet,R.M. (1993) Crystal structure of globular domain of histone H5 and its implications for nucleosome binding. *Nature*, **362**, 219–223

66. Aravind,L., Iyer,L.M. and Anantharaman,V. (2003) The two faces of Alba: the evolutionary connection between proteins participating in chromatin structure and RNA metabolism. *Genome Biol.*, **4**, R64.

67. Birney,E., Kumar,S. and Krainer,A.R. (1993) Analysis of the RNA-recognition motif and RS and RGG domains: conservation in metazoan pre-mRNA splicing factors. *Nucleic Acids Res.*, **21**, 5803–5816.

68. Intine,R.V., Tenenbaum,S.A., Sakulich,A.L., Keene,J.D. and Maraia,R.J. (2003) Differential phosphorylation and subcellular localization of La RNPs associated with precursor tRNAs and translation-related mRNAs. *Mol. Cell*, **12**, 1301–1307.

69. Linder,P. and Lasko,P. (2006) Bent out of shape: RNA unwinding by the DEAD-box helicase Vasa. *Cell*, **125**, 219–221.

70. Kim,C.A. and Bowie,J.U. (2003) SAM domains: uniform structure, diversity of function. *Trends Biochem. Sci.*, **28**, 625–628.

71. Green,J.B., Gardner,C.D., Wharton,R.P. and Aggarwal,A.K. (2003) RNA recognition via the SAM domain of Smaug. *Mol. Cell*, **11**, 1537–1548.

72. Yang,P., Fu,H., Walker,J., Papa,C.M., Smalle,J., Ju,Y.M. and Vierstra,R.D. (2004) Purification of the Arabidopsis 26S proteasome: biochemical and molecular analyses revealed the presence of multiple isoforms. *J. Biol. Chem.*, **279**, 6401–6413.

73. Ponting,C.P. (2002) Novel domains and orthologues of eukaryotic transcription elongation factors. *Nucleic Acids Res.*, **30**, 3643–3652.

74. Hunt,A.G., Xu,R., Addepalli,B., Rao,S., Forbes,K.P., Meeks,L.R., Xing,D., Mo,M., Zhao,H., Bandyopadhyay,A. *et al.* (2008) Arabidopsis mRNA polyadenylation machinery: comprehensive analysis of protein-protein interactions and gene expression profiling. *BMC Genomics*, **9**, 220.

75. Aravind,L. and Koonin,E.V. (2001) THUMP–a predicted RNA-binding domain shared by 4-thiouridine, pseudouridine synthases and RNA methylases. *Trends Biochem. Sci.*, **26**, 215–217.

76. Winter,D., Vinegar,B., Nahal,H., Ammar,R., Wilson,G.V. and Provart,N.J. (2007) An "Electronic Fluorescent Pictograph" browser for exploring and analyzing large-scale biological data sets. *PLoS One*, **2**, e718.

77. Belmonte,M.F., Kirkbride,R.C., Stone,S.L., Pelletier,J.M., Bui,A.Q., Yeung,E.C., Hashimoto,M., Fei,J., Harada,C.M., Munoz,M.D. *et al.* (2013) Comprehensive developmental profiles of gene activity in regions and subregions of the Arabidopsis seed. *Proc. Natl. Acad. Sci U.S.A.*, **110**, E435–E444.

78. Goldberg,R.B., de Paiva,G. and Yadegari,R. (1994) Plant embryogenesis: zygote to seed. *Science*, **266**, 605–614.

79. Teissere,M., Penon,P., van Huystee,R.B., Azou,Y. and Ricard,J. (1975) Hormonal control of transcription in higher plants. *Biochim. Biophys. Acta*, **402**, 391–402.

80. Guilfoyle,T.J., Lin,C.Y., Chen,Y.M., Nagao,R.T. and Key,J.L. (1975) Enhancement of soybean RNA polymerase I by auxin. *Proc. Natl. Acad. Sci. U.S.A.*, **72**, 69–72.

81. Chen,Y.M., Huang,D.H., Lin,S.F., Lin,C.Y. and Key,J.L. (1983) Fractionation of nucleoli from auxin-treated soybean hypocotyl into nucleolar chromatin and preribosomal particles. *Plant Physiol.*, **73**, 746–753.

82. Zheng,K., Wang,Y., Zhang,N., Jia,Q., Wang,X., Hou,C., Chen,J.G. and Wang,S. (2017) Involvement of PACLOBUTRAZOL RESISTANCE6/KIDARI, an atypical bHLH transcription factor, in auxin responses in Arabidopsis. *Front. Plant Sci.*, **8**, 1813.

83. Beta,R.A.A. and Balatsos,N.A.A. (2018) Tales around the clock: Poly(A) tails in circadian gene expression. *Wiley Interdiscip. Rev. RNA.*, e1484.

84. Martin,T., Oswald,O. and Graham,I.A. (2002) Arabidopsis seedling growth, storage lipid mobilization, and photosynthetic gene expression are regulated by carbon:nitrogen availability. *Plant Physiol.*, **128**, 472–481

85. Gerhardy,S., Menet,A.M., Peña,C., Petkowski,J.J. and Panse,V.G. (2014) Assembly and nuclear export of pre-ribosomal particles in budding yeast. *Chromosoma*, **123**, 327–344.

86. Leeds,N.B., Small,E.C., Hiley,S.L., Hughes,T.R. and Staley,J.P. (2006) The splicing factor Prp43p, a DEAH box ATPase, functions in ribosome biogenesis. *Mol. Cell Biol.*, **26**, 513–522.

87. Fleurdépine,S., Deragon,J.M., Devic,M., Guilleminot,J. and Bousquet-Antonelli,C. (2007) A bona fide La protein is required for embryogenesis in *Arabidopsis thaliana*. *Nucleic Acids Res.*, **35**, 3306–3321.

88. Cui,Y., Rao,S., Chang,B., Wang,X., Zhang,K., Hou,X., Zhu,X., Wu,H., Tian,Z., Zhao,Z. *et al.* (2015) AtLa1 protein initiates IRES-dependent translation of WUSCHEL mRNA and regulates the stem cell homeostasis of Arabidopsis in response to environmental hazards. *Plant Cell Environ.*, **38**, 2098–2114.

89. Kruszka,K., Barneche,F., Guyot,R., Ailhas,J., Meneau,I., Schiffer,S., Marchfelder,A. and Echeverría,M. (2003) Plant dicistronic tRNA-snoRNA genes: a new mode of expression of the small nucleolar RNAs processed by RNase Z. *EMBO J.*, **22**, 621–632.

90. Uhrig,J.F., Canto,T., Marshall,D. and MacFarlane,S.A. (2004) Relocalization of nuclear ALY proteins to the cytoplasm by the tomato bushy stunt virus P19 pathogenicity protein. *Plant Physiol.*, **135**, 2411–2423.

91. Hang,R., Liu,C., Ahmad,A., Zhang,Y., Lu,F. and Cao,X. (2014) Arabidopsis protein arginine methyltransferase 3 is required for ribosome biogenesis by affecting precursor ribosomal RNA processing. *Proc. Natl. Acad. Sci. U.S.A.*, **111**, 16190–16295.

92. Okanami,M., Meshi,T. and Iwabuchi,M. (1998) Characterization of a DEAD box ATPase/RNA helicase protein of *Arabidopsis thaliana*. *Nucleic Acids Res.*, **26**, 2638–2643.

93. Du,J., Gao,Y., Zhan,Y., Zhang,S., Wu,Y., Xiao,Y., Zou,B., He,K., Gou,X., Li,G. *et al.* (2016) Nucleocytoplasmic trafficking is essential for BAK1- and BKK1-mediated cell-death control. *Plant J.*, **85**, 520–531.

94. Takeno,K. (2016) Stress-induced flowering: the third category of flowering response. *J. Exp. Bot.*, **67**, 4925–4934.

95. Borisjuk,L., Walenta,S., Weber,H., Mueller-Klieser,W. and Wobus,U. (1998) High-resolution histographical mapping of glucose concentrations in developing cotyledons of Vicia faba in relation to mitotic activity and storage processes: glucose as a possible developmental trigger. *Plant J.*, **15**, 583–591.

96. Hsu,Y.F., Chen,Y.C., Hsiao,Y.C., Wang,B.J., Lin,S.Y., Cheng,W.H., Jauh,G.Y., Harada,J.J. and Wang,C.S. (2014) AtRH57, a DEAD-box RNA helicase, is involved in feedback inhibition of glucose-mediated abscisic acid accumulation during seedling development and additively affects pre-ribosomal RNA processing with high glucose. *Plant J.*, **77**, 119–135.

97. Rook,F., Hadingham,S.A., Li,Y. and Bevan,M.W. (2006) Sugar and ABA response pathways and the control of gene expression. *Plant Cell Environ.*, **29**, 426–434.

98. Munns,R. and Tester,M. (2008) Mechanisms of salinity tolerance. *Ann. Rev. Plant Biol.*, **59**, 651–681

99. Kosová,K., Vítámvás,P., Prášil,I.T. and Renaut,J. (2011) Plant proteome changes under abiotic stress–contribution of proteomics studies to understanding plant stress response. *J. Proteomics.*, **74**, 1301–1322.